

# Thermal Hall Effect in the Kitaev-Heisenberg System with Spin-Phonon Coupling

Shaozhi Li\* and Satoshi Okamoto

*Materials Science and Technology Division, Oak Ridge National Laboratory, Oak Ridge, TN 37831, USA*

(Dated: December 14, 2021)

We investigate the thermal Hall effect in a Kitaev-Heisenberg system, a model for Kitaev candidate  $\alpha$ -RuCl<sub>3</sub>, in the presence of the coupling between spin and phonon arising from chlorine atoms' vibration. We observe that the coupling modifies the relative stability between different magnetic states under a magnetic field, especially stabilizing a canted zigzag antiferromagnetic state. Remarkably, the spin-phonon interaction has distinct effects on the thermal Hall conductivity in different magnetically ordered states. For the canted zigzag state, which is relevant to  $\alpha$ -RuCl<sub>3</sub>, the spin-phonon interaction enhances the energy gap that is induced by a magnetic field and suppresses the thermal Hall conductivity at low temperatures. Qualitatively similar results are also observed in the extended Kitaev-Heisenberg model that was proposed for  $\alpha$ -RuCl<sub>3</sub>. Our results demonstrate a crucial role of phonon degrees of freedom to the thermal Hall effect in Kitaev materials.

*Introduction.* Phonons play an essential role in shaping electronic and magnetic properties in materials [1–5, 7–13]. For example, the electron-phonon interaction induces the charge-density-wave and superconductivity in the high-temperature superconductor Ba<sub>0.51</sub>K<sub>0.49</sub>BiO<sub>3</sub> [6]. Besides, phonons can couple to spins and induce the spin-Peierls transition in quasi-one-dimensional materials, including CuGeO<sub>3</sub> [14] and Ti-OCl [15].

Recently, a significant interplay between phonons and spins was observed in the Kitaev material  $\alpha$ -RuCl<sub>3</sub> [16–27]. In  $\alpha$ -RuCl<sub>3</sub>, the edge-sharing Ru-Cl octahedra form a honeycomb lattice with an effective spin-1/2. The interaction between two nearest-neighbor pseudospins strongly depends on the Ru-Ru distance and the Ru-Cl-Ru bond angle [28]. In  $\alpha$ -RuCl<sub>3</sub>, both the spin and phonon behaviors are modified by the spin-phonon interaction. For example, the spin-phonon coupling renormalizes phonon propagators and generates the salient Fano lineshape in the Raman spectroscopy [18, 29–32]. Besides, the coupling of phonons to Majorana fermions plays a pivotal role in realizing the quantum thermal Hall effect in  $\alpha$ -RuCl<sub>3</sub> [33–38].

To gain insight into the novel magnetic behavior in  $\alpha$ -RuCl<sub>3</sub>, various theoretical models were developed by using the density-functional theory (DFT) or fitting to inelastic neutron scattering spectra [16, 19, 39–47]. Although the spin-phonon interaction is not included, these models generate a number of experimentally related predictions, including the heat capacity and the Raman spectroscopy. However, some important experimental features remained unexplained, such as the Fano effect in the Raman spectroscopy [31, 32] and the sample dependence of the quantized thermal Hall effect in  $\alpha$ -RuCl<sub>3</sub> [48]. It has been proposed that the spin-phonon coupling is essential to resolve these difficulties. In this case, it is necessary to develop a model that includes both spin and phonon degrees of freedoms. However, compared to the Kitaev-Heisenberg model, far fewer studies exist for such a model. Recently, several stud-

ies have considered phonons in the Majorana fermion representation to explain the Fano effect [31, 32, 37]. Such studies only considered the Kitaev-type interaction and neglected some significant spin-spin interactions in  $\alpha$ -RuCl<sub>3</sub>. Furthermore, the effect of the spin-phonon coupling on the thermal Hall conductivity has not been clarified, although some interesting predictions have been made by analyzing a phenomenology model [49].

In this work, we develop a microscopic model with a spin-phonon interaction to study the thermal Hall conductivity in  $\alpha$ -RuCl<sub>3</sub>. We consider the optical phonon, which originates from the vibration of the Cl-Cl bond (shown in Fig. 1(a)). This optical phonon modifies the Ru-Cl-Ru bond angle, hereby the spin-spin interaction between Ru atoms [28, 50]. We first use the mean-field theory to study the spin-phonon interaction in the Kitaev-Heisenberg model under a magnetic field. We observe that optical phonons stabilize the canted zigzag state and destabilize the antiferromagnetic star state. Next, we use the generalized spin-wave theory to study the thermal Hall conductivity. We find that the spin-phonon interaction has distinct effects on the thermal Hall conductivity in different magnetic states. For example, in the canted zigzag state, which is relevant to  $\alpha$ -RuCl<sub>3</sub>, the spin-phonon interaction increases the energy gap and suppresses the thermal Hall conductivity at low temperatures. These results are also observed in the extended-Kitaev-Heisenberg model, which was proposed to describe  $\alpha$ -RuCl<sub>3</sub>. In other magnetic states, i.e. the antiferromagnetic star state, the spin-phonon interaction decreases both the energy gap and the Berry curvature density in the low-energy regime. Because these two effects compete with each other, a nonmonotonic behavior appears in the thermal Hall conductivity. Our results provide *qualitative* guidance to understand the thermal Hall conductivity in  $\alpha$ -RuCl<sub>3</sub> under a low magnetic field, where long-range magnetic ordering remains.

*Model Hamiltonian.* The optical mode of the chlorine atom's motion in  $\alpha$ -RuCl<sub>3</sub> is shown in Fig. 1 (a). This optical phonon changes the distance  $d$  between two chlo-

rine atoms, resulting in modifying the spin-spin interaction  $J(d)$  between Ru atoms. Assuming the variation of  $d$  is small, the interaction can be approximated as  $J(d) = J(d_0)[1 - g(d - d_0)]$ , where  $d_0$  is the distance at the equilibrium position, and the spin-phonon coupling  $g = -\frac{1}{J(d_0)} \frac{\partial J(d)}{\partial d}$ . In this case, the proposed extended-Kitaev-Heisenberg model [51] for  $\alpha$ -RuCl<sub>3</sub> may be modified as  $H = H_{\text{spin}} + H_{\text{ph}} + H_{\text{spin-ph}}$ , where

$$\begin{aligned} H_{\text{spin}} &= \sum_{\langle ij \rangle_\gamma} \left[ 2K_1 \hat{S}_i^\gamma \hat{S}_j^\gamma + \Gamma (\hat{S}_i^\alpha \hat{S}_j^\beta + \hat{S}_i^\beta \hat{S}_j^\alpha) \right. \\ &\quad \left. + J_1 \hat{\mathbf{S}}_i \cdot \hat{\mathbf{S}}_j \right] + J_3 \sum_{\langle\langle ij \rangle\rangle} \hat{\mathbf{S}}_i \cdot \hat{\mathbf{S}}_j - \sum_{i,\alpha} H_\alpha \hat{S}_i^\alpha, \\ H_{\text{ph}} &= \sum_{\langle ij \rangle} \left[ \frac{M \hat{u}_{ij}^2}{2} + \frac{K \hat{u}_{ij}^2}{2} \right], \\ H_{\text{spin-ph}} &= - \sum_{\langle ij \rangle_\gamma} g \hat{u}_{ij} \left[ 2K_1 \hat{S}_i^\gamma \hat{S}_j^\gamma + J_1 \hat{\mathbf{S}}_i \cdot \hat{\mathbf{S}}_j + \Gamma (\hat{S}_i^\alpha \hat{S}_j^\beta + \hat{S}_i^\beta \hat{S}_j^\alpha) \right]. \end{aligned}$$

Here,  $J_{1(3)}$  is the nearest-neighbor (third-nearest-neighbor) Heisenberg coupling;  $K_1$  and  $\Gamma$  are the nearest-neighbor Kitaev and symmetric off-diagonal couplings, respectively.  $\langle ij \rangle_\gamma$  denotes the nearest-neighbor  $\gamma$  bond, with  $\gamma = x, y, z$ , and  $\langle\langle ij \rangle\rangle$  denotes the third-nearest neighbor bond.  $(\alpha, \beta, \gamma) = (y, z, x), (z, x, y)$ , and  $(x, y, z)$  for the  $x, y$ , and  $z$  bonds, respectively. We follow Ref. [52] and set that the [111] direction in the spin space is parallel to the  $c$  axis and  $S^z$  direction is on the  $ac$  plane.  $H_\alpha$  is the magnetic field along the  $\alpha$  direction, which is shown in Fig. 1(b). The magnetic field strength is labeled as  $|\mathbf{H}| = \sqrt{H_a^2 + H_b^2 + H_c^2}$ .  $\hat{u}_{ij}$  denotes the displacement operator of the Cl-Cl bond, and  $\langle \hat{u}_{ij} \rangle = d_{ij} - d_0$ .  $M$  and  $K$  are the mass of the chlorine atom and the elastic constant between chlorine atoms, respectively.

The ground state is obtained using the mean-field approach [52, 53]. Specifically, we set  $\hat{S}^\gamma = \langle S^\gamma \rangle + \delta \hat{S}^\gamma$  and  $\hat{u} = \langle u \rangle + \delta \hat{u}$ . The Hamiltonian is then rewritten as  $H = \text{const} + H^{(1)} + H^{(2)} + H^{(3)}$ , where  $H^{(1)}$ ,  $H^{(2)}$ , and  $H^{(3)}$  include terms with one, two, and three operators, respectively.  $\langle S^\gamma \rangle$  and  $\langle u \rangle$  are obtained by self-consistently solving  $H^{(1)}$  (see supplementary [53]). After obtaining stable spin and lattice configurations, we apply a generalized spin-wave theory to  $H^{(2)}$  and compute the Berry curvature [53]. The thermal Hall conductivity is then calculated via  $\kappa_{xy} = -\frac{k_B T}{\hbar N} \sum_k^{BZ} \sum_{n=1}^L c_2(f_{\text{BE}}(\epsilon_{nk})) \Omega_{nk}$  [54, 55], where  $c_2(x)$  is given by  $c_2(x) = \int_0^x dt (\ln \frac{1+t}{t})^2$ ,  $f_{\text{BE}}(\epsilon_{nk})$  is the Bose distribution function, and  $BZ$  denotes the Brillouin zone.  $\Omega_{nk}$  is the Berry curvature at the momentum  $k$  for the  $n$ th band.  $2L$  is the number of bands, and  $N$  is the number of the magnetic unit cell, which is labeled as a dashed-rectangular in the inset of Fig. 1. In this work, we set  $N = 120 \times 120$ ,  $\hbar = k_B = 1$  and neglect three-particle interaction  $H^{(3)}$ .

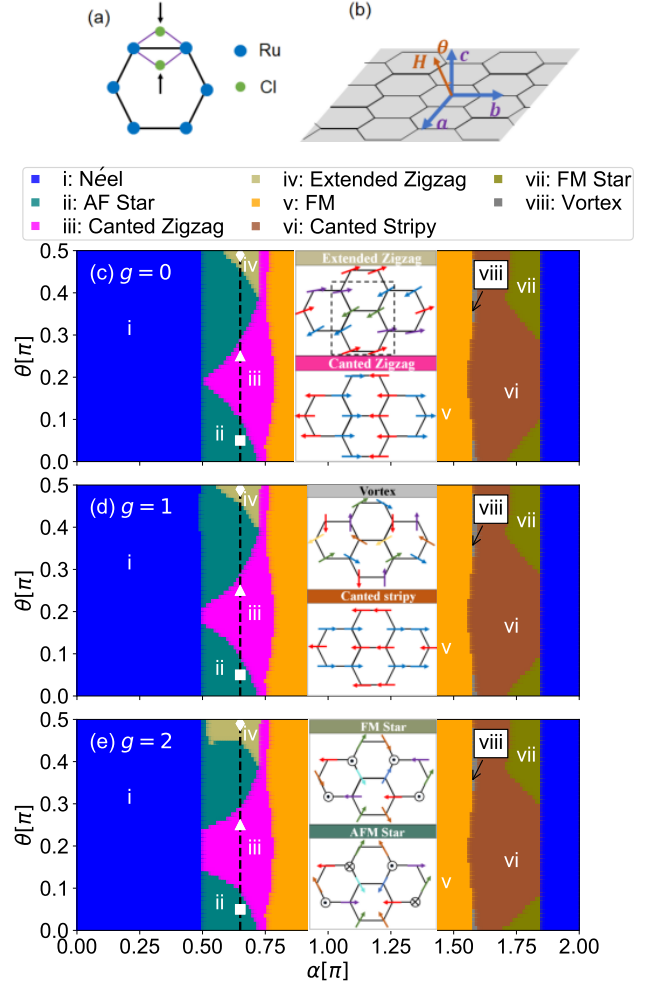


FIG. 1. (a) A sketch of chlorine atoms' vibration in  $\alpha$ -RuCl<sub>3</sub>. (b) A sketch of the Honeycomb lattice that lies on the  $ab$  plane. Panels (c)-(d) plot the phase diagrams for the spin-phonon interaction  $g = 0, 1$ , and  $2$  under a magnetic field  $|\mathbf{H}| = 0.4A$ , respectively. The insets in panels (c)-(e) show the spin configuration of each magnetic state when the magnetic field is along the  $c$  axis. The spin configuration is projected onto the  $ab$  plane.

**Results.** Considering a recent experiment on  $\alpha$ -RuCl<sub>3</sub> [26], we set the phonon frequency  $\omega_{\text{ph}} = 8$  meV, hereby the elastic constant  $K = 535.2$  meV/ $\text{\AA}^2$ . We first study this model with  $\Gamma = 0$  and  $J_3 = 0$ . In this case, we set  $K_1 = A \cos \alpha$ ,  $J_1 = A \sin \alpha$  [52, 56–58], and  $A = \omega_{\text{ph}}$ . At zero field, the ground state of the classical model is the Néel state for  $-0.15\pi < \alpha < 0.5\pi$ , the zigzag state for  $0.5\pi < \alpha < 0.85\pi$ , the ferromagnetic (FM) state for  $0.85\pi < \alpha < 1.5\pi$ , and the stripy state for  $1.5\pi < \alpha < 1.85\pi$  [53, 56]. These ground states are changed under a magnetic field [52, 56]. In this work, we rotate the magnetic field in the  $ac$  plane (shown in Fig. 1(b)) and label the angle between the magnetic field and the  $c$  axis as  $\theta$ . Figure 1(c) shows the phase diagram in the plane of  $\alpha$  and  $\theta$  at  $|\mathbf{H}| = 0.4A$  and  $g = 0$ . Besides these four magnetic

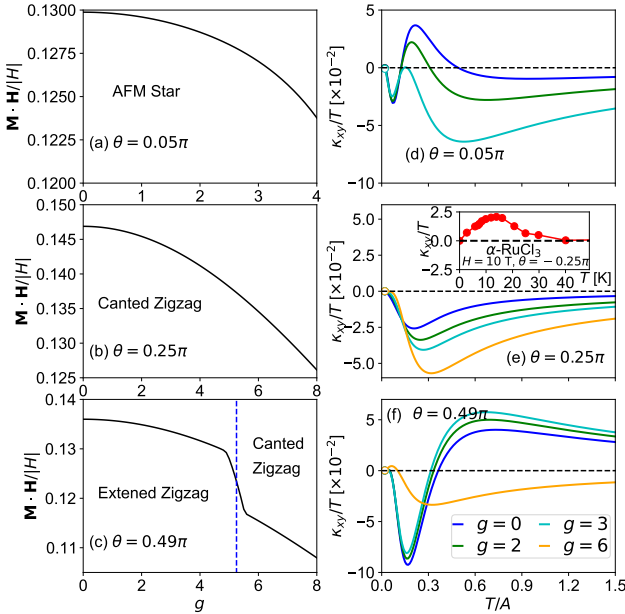


FIG. 2. The left column shows the magnetization  $\mathbf{M} \cdot \mathbf{H}/|\mathbf{H}|$  along the field direction for three different values of  $\theta$ . The blue dashed line in panel (c) represents the phase boundary between the extended zigzag and canted zigzag states. The right column shows the corresponding thermal Hall conductivity  $\kappa_{xy}/T$  as a function of temperature  $T$ . The inset in panel (e) plots the thermal Hall conductivity of  $\alpha$ -RuCl<sub>3</sub>, obtained from Ref. [59]. Here, we set  $\alpha = 0.65\pi$  and  $|\mathbf{H}| = 0.4A$ .

states, there appear another four magnetic states, including anti-ferromagnetic star state (AF Star), extended zigzag state, ferromagnetic star state (FM Star), and vortex state (vortex) [52, 53, 56]. Remarkably, the spin-phonon interaction changes the magnetic ground state and modifies the phase diagram. As shown in Figs 1(d) and 1(e), the spin-phonon interaction increases the regions of the canted zigzag and extended zigzag states by suppressing the AF Star state when  $0.5\pi < \alpha < 0.75\pi$ . By further increasing the spin-phonon interaction, the extended zigzag state is replaced by the canted zigzag state (see Fig. 2). These results imply that optical phonons stabilize the zigzag state under a magnetic field.

We now analyze the effect of the spin-phonon interaction on the magnetization  $\mathbf{M}$  and the thermal Hall conductivity  $\kappa_{xy}$  in the parameter region of the zigzag state that exists at zero field. If not stated otherwise, we set  $\alpha = 0.65\pi$  and  $|\mathbf{H}| = 0.4A$  in this work. The value  $\alpha = 0.65\pi$  is labeled by the dashed line in Figs. 1 (c) - 1 (e). Figures 2(a) - 2(c) plot the magnetization for  $\theta = 0.05\pi$ ,  $0.25\pi$ , and  $0.49\pi$ , respectively. The ground states for these three values of  $\theta$  are the AFM Star, canted zigzag, and extended zigzag states, labeled as a white square, triangle, and diamond in Figs. 1 (c) - 1(e), respectively. Figures 2(a) - 2(c) show that the spin-phonon interaction suppresses the magnetization for all these three states. In addition, a first-order phase transition from the

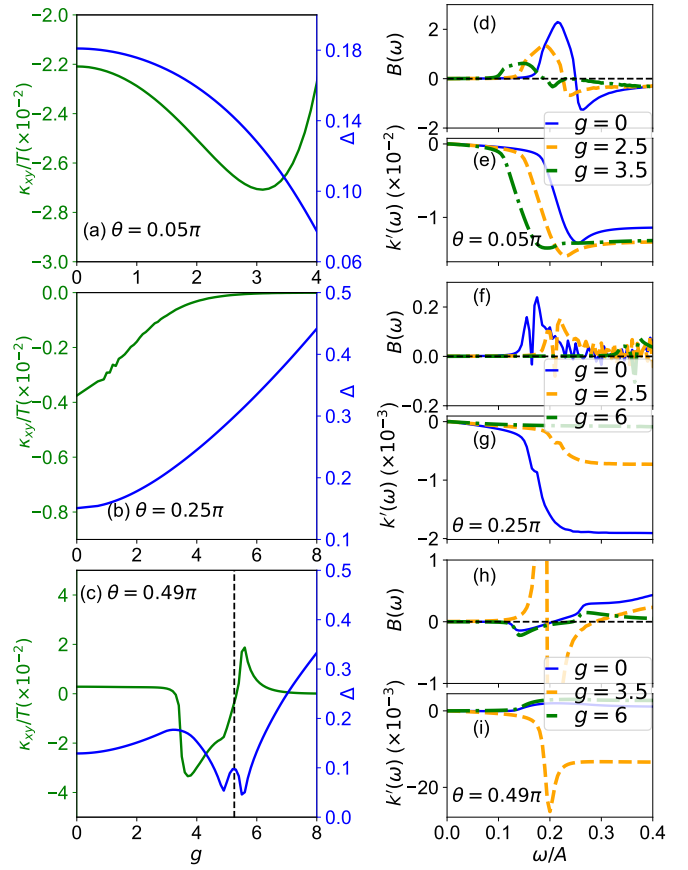


FIG. 3. The left column plots the thermal Hall conductivity  $\kappa_{xy}/T$  (green curve) and the energy gap  $\Delta$  (blue curve) as a function of the spin-phonon interaction  $g$  for three different values of  $\theta$ . The black dashed line in panel (c) represents the phase boundary between the extended zigzag state and the canted zigzag state. Panels (d), (f), and (h) plot the Berry curvature density  $B(\omega)$ , and panels (e), (g), and (i) plot the integrated Berry curvature density  $K'(\omega)$ . Here, we set  $\alpha = 0.65\pi$ ,  $T = 0.04A$ , and  $|\mathbf{H}| = 0.4A$ .

extended zigzag state to the canted zigzag state occurs at  $\theta = 0.49\pi$  and  $g = 5.6$ , accompanied by a sudden drop in  $\mathbf{M} \cdot \mathbf{H}/|\mathbf{H}|$ .

Figures 2(d) - 2(f) plot the thermal Hall conductivity  $\kappa_{xy}/T$  as a function of temperature  $T$  for several different values of  $g$ . Interestingly,  $\kappa_{xy}/T$  has distinct temperature dependences in different magnetic states. We examine  $\kappa_{xy}/T$  at various values of  $\alpha$  and find that  $\kappa_{xy}/T$  has three and two extrema in the AFM Star and extended zigzag states, respectively.  $\kappa_{xy}/T$  could have either one or two extrema in the canted zigzag state, depending on the value of  $\alpha$ . While it is challenging to quantitatively compare to experiments, we note that the temperature-dependent  $\kappa_{xy}/T$  in the canted zigzag state is qualitatively consistent with that measured in  $\alpha$ -RuCl<sub>3</sub> [59] (see the inset of Fig. 2(e)).  $\kappa_{xy}/T$  in the intermediate temperature regime ( $1.2A > T > 0.3 A$ ) has been significantly changed by the spin-phonon interaction for all

these three states. Recently, it was proposed that  $\kappa_{xy}/T$  in the intermediate temperature regime exhibits the universal scaling with the exponential form  $e^{-T/T_0}$ , where  $T_0$  is proportional to the bandwidth [60]. While our results also show a similar universal behavior in the intermediate temperature regime, the change in  $\kappa_{xy}/T$  arises from the change in the energy gap and the Berry curvature, rather than the bandwidth.

To better visualize the change in  $\kappa_{xy}/T$  at low temperatures, we plot  $\kappa_{xy}/T$  in Figs. 3(a) - 3(c) for  $T = 0.04A$ . The energy gap  $\Delta$  (blue curve) is also plotted in these three panels. At  $\theta = 0.05\pi$  (AF Star),  $|\kappa_{xy}|/T$  is enhanced by the spin-phonon coupling when  $g < 3$  and suppressed when  $g > 3$ . This nonmonotonic behavior arises from the competition between the changes in  $\Delta$  and  $\Omega_{n,k}$ . The latter contribution can be visualized more clearly by the Berry curvature density, which is defined as  $B(\omega) = \sum_{n,k} \Omega_{n,k} \delta(\omega - \epsilon_{n,k})$  and plotted in Figs. 3(d), 3(f), and 3(h). The  $\delta$  function is evaluated using the Lorentzian function with a width of 0.005. In the AF Star state, the spin-phonon interaction monotonically decreases  $\Delta$ , leading to an enhancement of  $|\kappa_{xy}|/T$ . However, the Berry curvature density near  $\omega = 0.2A$  is suppressed by the spin-phonon interaction, resulting in the decrease in  $|\kappa_{xy}|/T$ . Figure 3(e) plots the integrated Berry curvature density  $K'(\omega) = -\int_0^\omega c_2(f_{BE}(\omega'))B(\omega')d\omega'$ , equivalent to the thermal Hall conductivity. It is easy to observe this competition from  $K'(\omega)$  in Fig. 3(e). At  $\theta = 0.25\pi$  (canted zigzag),  $|\kappa_{xy}|/T$  is suppressed by the spin-phonon interaction because  $\Delta$  increases and  $B(\omega \approx 0.2A)$  decreases with  $g$ .

At  $\theta = 0.49\pi$ ,  $\kappa_{xy}/T$  is positive and slightly suppressed by  $g$  when  $g < 3$ . This behavior is attributed to the enhanced energy gap. Near  $g = 3.2$ ,  $\kappa_{xy}/T$  suddenly becomes negative and increases with  $g$ . This sudden change is due to the band crossing at the  $\Gamma$  point (see supplementary [53]). Specifically, the energy gap  $\Delta'$  between the lowest and second-lowest magnon bands at the  $\Gamma$  point decreases as  $g$  increases. At  $g = 3.2$ ,  $\Delta'$  approaches zero, and the sign of  $\Omega_{1,\Gamma}$  and  $\Omega_{2,\Gamma}$  swaps. By further increasing  $g$ ,  $\Delta'$  increases. At  $g = 5.6$ , the phase transition occurs, and the ground state becomes the canted zigzag state.  $|\kappa_{xy}|/T$  in this canted zigzag state has the same behavior as that shown in Fig. 3(b).

Our results show that the optical phonons significantly change the thermal Hall conductivity in the Kitaev-Heisenberg system. The change in  $\kappa_{xy}$  arises from two origins. First, the interaction strength  $J_{ij}$  is modified by  $g\hat{u}_{ij}$ . In our calculations, the maximal value of  $\langle \hat{u}_{ij} \rangle$  is about 0.01 Å at  $g = 8$ , which is comparable to the DFT prediction [28]. Second, the magnon-phonon coupling, existing in  $H^{(2)}$ , changes the eigenstate, hereby the Berry curvature. To distinguish the contribution of each factor to  $\kappa_{xy}$ , we diagonalize the Hamiltonian  $H'$  without the spin-phonon scattering. Figure 4 plots the

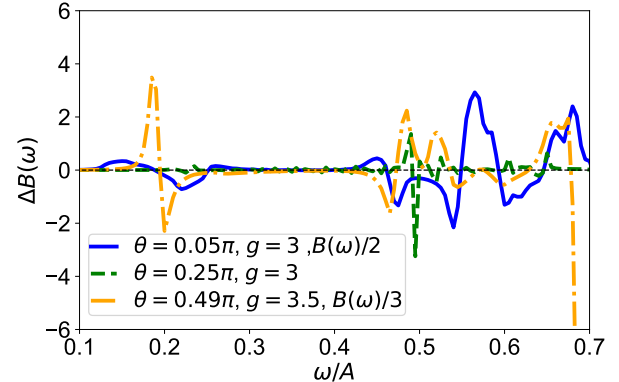


FIG. 4. The difference  $\Delta B(\omega)$  between the Berry curvature density  $B(\omega)$  of the Hamiltonian with and without spin-phonon scatterings. Here, we set  $\alpha = 0.65\pi$  and  $|\mathbf{H}| = 0.4A$ .

difference  $\Delta B(\omega)$  between the Berry curvature density of the Hamiltonian with and without spin-phonon scatterings. At  $\theta = 0.05\pi$  (AFM Star state) and  $\theta = 0.49\pi$  (extended zigzag state),  $\Delta B(\omega \approx 0.2A) \neq 0$ , implying that the spin-phonon scattering changes the low temperature thermal Hall conductivity in both AFM Star and extended zigzag states. Besides, the band crossing at  $\theta = 0.49\pi$  and  $g = 3.2$  does not occur when the spin-phonon scattering is removed. At  $\theta = 0.25\pi$  (canted zigzag),  $\Delta B(\omega)$  is nonzero when  $\omega > 0.4A$ , implying that the spin-phonon scattering changes  $\kappa_{xy}$  in the intermediate temperature regime in the canted zigzag state.

Finally, we study the extended Kitaev-Heisenberg model with  $J_1 = -0.5$  meV,  $K_1 = -5.0$  meV,  $\Gamma = 2.5$  meV,  $J_3 = 0.5$  meV and  $|\mathbf{H}| = 0.8$  meV, which has been applied to analyze the experimentally observed anisotropy in  $\alpha$ -RuCl<sub>3</sub> [40, 61–65]. Due to the off-diagonal and the third nearest-neighbor interactions, the canted zigzag ground state does not change as we rotate the magnetic field. The spin-phonon interaction enhances the energy gap and suppresses the thermal Hall conductivity at  $T = 3.52$  K in this state (see supplementary [53]). This result is consistent with that observed in the Kitaev-Heisenberg model at  $\theta = 0.25\pi$  and  $|\mathbf{H}| = 0.4A$  (canted zigzag state).

*Summary.* In this work, we studied the effect of the spin-phonon interaction on the magnetic ground state and the thermal Hall conductivity in the Kitaev-Heisenberg system. We observed that a large spin-phonon interaction stabilizes the canted zigzag state under a magnetic field. Further, the spin-phonon interaction has distinct effects on the thermal Hall conductivity in different magnetic states. In the zigzag state, the spin-phonon interaction increases the energy gap and suppresses the low temperature thermal Hall conductivity. A qualitatively similar effect is also observed in a more realistic model (extended-Kitaev-Heisenberg model) for  $\alpha$ -RuCl<sub>3</sub>. Thus this effect is independent of the model

and parameters in the zigzag state. If this effect is also held in the spin liquid state, the spin-phonon interaction stabilizes the topological properties in  $\alpha$ -RuCl<sub>3</sub>. Our results provide crucial guidance to understand thermal Hall conductivity in Kitaev materials, including  $\alpha$ -RuCl<sub>3</sub> and Na<sub>2</sub>Co<sub>2</sub>TeO<sub>6</sub> [66].

In this work, we consider optical phonons arising from the displacement of chlorine atoms. It would be important to study acoustic phonons, which involve the displacement of Ruthenium atoms, and examine how these phonons modify the magnetic properties in  $\alpha$ -RuCl<sub>3</sub>.

This research was supported by the U.S. Department of Energy, Office of Science, National Quantum Information Science Research Centers, Quantum Science Center. This research used resources of the Compute and Data Environment for Science (CADES) at the Oak Ridge National Laboratory, which is supported by the Office of Science of the U.S. Department of Energy under Contract No. DE-AC05-00OR22725.

---

\* lis1@ornl.gov

- [1] W. Weber, Phys. Rev. Lett. **58**, 1371 (1987).
- [2] D. J. J. Marchand, G. De Filippis, V. Cataudella, M. Berciu, N. Nagaosa, N. V. Prokof'ev, A. S. Mishchenko, and P. C. E. Stamp, Phys. Rev. Lett. **105**, 266605 (2010).
- [3] J. Sous, M. Chakraborty, R. V. Krems, and M. Berciu, Phys. Rev. Lett. **121**, 247001 (2018).
- [4] S. Li and S. Johnston, npj Quantum Materials **5**, 40 (2020).
- [5] B. Xing, W.-T. Chiu, D. Poletti, R. T. Scalettar, and G. Batrouni, Phys. Rev. Lett. **126**, 017601 (2021).
- [6] C. H. P. Wen, H. C. Xu, Q. Yao, R. Peng, X. H. Niu, Q. Y. Chen, Z. T. Liu, D. W. Shen, Q. Song, X. Lou, Y. F. Fang, X. S. Liu, Y. H. Song, Y. J. Jiao, T. F. Duan, H. H. Wen, P. Dudin, G. Kotliar, Z. P. Yin, and D. L. Feng, Phys. Rev. Lett. **121**, 117002 (2018).
- [7] M. Lazzeri, C. Attaccalite, L. Wirtz, and F. Mauri, Phys. Rev. B **78**, 081406(R) (2008).
- [8] E. A. Nowadnick, S. Johnston, B. Moritz, R. T. Scalettar, and T. P. Devereaux, Phys. Rev. Lett. **109**, 246404 (2012).
- [9] S. Li, E. Khatami, and S. Johnston, Phys. Rev. B **95**, 121112(R) (2017).
- [10] N. C. Costa, K. Seki, S. Yunoki, and S. Sorella, Communications Physics **3**, 80 (2020).
- [11] N. C. Costa, K. Seki, and S. Sorella, Phys. Rev. Lett. **126**, 107205 (2021).
- [12] C.-C. Lee, J.-Y. Chiu, Y. Yamada-Takamura, and T. Ozaki, Phys. Rev. B **104**, 064114 (2021).
- [13] A. Sapkota, T. C. Sterling, P. M. Lozano, Y. Li, H. Cao, V. O. Garlea, D. Reznik, Q. Li, I. A. Zaliznyak, G. D. Gu, and J. M. Tranquada, Phys. Rev. B **104**, 014304 (2021).
- [14] M. Hase, I. Terasaki, and K. Uchinokura, Phys. Rev. Lett. **70**, 3651 (1993).
- [15] M. Shaz, S. van Smaalen, L. Palatinus, M. Hoinkis, M. Klemm, S. Horn, and R. Claessen, Phys. Rev. B **71**, 100405(R) (2005).
- [16] K. W. Plumb, J. P. Clancy, L. J. Sandilands, V. V. Shankar, Y. F. Hu, K. S. Burch, H.-Y. Kee, and Y.-J. Kim, Phys. Rev. B **90**, 041112(R) (2014).
- [17] Y. Kubota, H. Tanaka, T. Ono, Y. Narumi, and K. Kindo, Phys. Rev. B **91**, 094422 (2015).
- [18] L. J. Sandilands, Y. Tian, K. W. Plumb, Y.-J. Kim, and K. S. Burch, Phys. Rev. Lett. **114**, 147201 (2015).
- [19] R. D. Johnson, S. C. Williams, A. A. Haghimirad, J. Singleton, V. Zapf, P. Manuel, I. I. Mazin, Y. Li, H. O. Jeschke, R. Valentí, and R. Coldea, Phys. Rev. B **92**, 235119 (2015).
- [20] J. A. Sears, M. Songvilay, K. W. Plumb, J. P. Clancy, Y. Qiu, Y. Zhao, D. Parshall, and Y.-J. Kim, Phys. Rev. B **91**, 144420 (2015).
- [21] H. B. Cao, A. Banerjee, J.-Q. Yan, C. A. Bridges, M. D. Lumsden, D. G. Mandrus, D. A. Tennant, B. C. Chakoumakos, and S. E. Nagler, Phys. Rev. B **93**, 134423 (2016).
- [22] A. Koitzsch, C. Habenicht, E. Müller, M. Knupfer, B. Büchner, H. C. Kandpal, J. van den Brink, D. Nowak, A. Isaeva, and T. Doert, Phys. Rev. Lett. **117**, 126403 (2016).
- [23] M. G. Yamada, H. Fujita, and M. Oshikawa, Phys. Rev. Lett. **119**, 057202 (2017).
- [24] Y. Kasahara, T. Ohnishi, Y. Mizukami, O. Tanaka, S. Ma, K. Sugii, N. Kurita, H. Tanaka, J. Nasu, Y. Motome, T. Shibauchi, and Y. Matsuda, Nature **559**, 227 (2018).
- [25] R. Henrich, A. U. B. Wolter, X. Zotos, W. Brenig, D. Nowak, A. Isaeva, T. Doert, A. Banerjee, P. Lampen-Kelley, D. G. Mandrus, S. E. Nagler, J. Sears, Y.-J. Kim, B. Büchner, and C. Hess, Phys. Rev. Lett. **120**, 117204 (2018).
- [26] H. Li, T. T. Zhang, A. Said, G. Fbbris, D. G. Mazzzone, Q. J. Yan, D. B. Mandrus, G. Halász, S. Okamoto, M. P. M. Dean, H. N. Lee, and H. Miao, Nature Communications **12**, 3513 (2021).
- [27] S. Mu, K. D. Dixit, W. Xiaoping, D. L. Abernathy, H. Cao, S. E. Nagler, P. Yan Jiaqiang, Lampen-Kelley, D. Mandrus, C. A. Polanco, L. Liang, G. B. Halász, Y. Cheng, A. Banerjee, and T. Berlijn, “The role of the third dimension in searching majorana fermions in  $\alpha$ -RuCl<sub>3</sub> via phonons,” ArXiv: 2111.07390 (2021).
- [28] H.-S. Kim and H.-Y. Kee, Phys. Rev. B **93**, 155143 (2016).
- [29] G. Li, X. Chen, Y. Gan, F. Li, M. Yan, F. Ye, S. Pei, Y. Zhang, L. Wang, H. Su, J. Dai, Y. Chen, Y. Shi, X. Wang, L. Zhang, S. Wang, D. Yu, F. Ye, J.-W. Mei, and M. Huang, Phys. Rev. Materials **3**, 023601 (2019).
- [30] A. Glamazda, P. Lemmens, S.-H. Do, Y. S. Kwon, and K.-Y. Choi, Phys. Rev. B **95**, 174429 (2017).
- [31] K. Feng, S. Swarup, and N. B. Perkins, “Footprints of the kitaev spin liquid in the fano lineshapes of the raman active optical phonons,” ArXiv: 2108.08878 (2021).
- [32] A. Metavitsiadis, W. Natori, J. Knolle, and W. Brenig, “Optical phonons coupled to kitaev spin liquid,” ArXiv: 2103.0982 (2021).
- [33] M. Ye, G. B. Halász, L. Savary, and L. Balents, Phys. Rev. Lett. **121**, 147201 (2018).
- [34] Y. Vinkler-Aviv and A. Rosch, Phys. Rev. X **8**, 031032 (2018).
- [35] A. Metavitsiadis and W. Brenig, Phys. Rev. B **101**, 035103 (2020).

- [36] M. Ye, R. M. Fernandes, and N. B. Perkins, Phys. Rev. Research **2**, 033180 (2020).
- [37] K. Feng, M. Ye, and N. B. Perkins, Phys. Rev. B **103**, 214416 (2021).
- [38] A. Ruiz, N. P. Breznay, M. Li, I. Rousochatzakis, A. Allen, I. Zinda, V. Nagarajan, G. Lopez, Z. Islam, M. H. Upton, J. Kim, A. H. Said, X.-R. Huang, T. Gog, D. Casa, R. J. Birgeneau, J. D. Koralek, J. G. Analytis, N. B. Perkins, and A. Frano, Phys. Rev. B **103**, 184404 (2021).
- [39] H.-S. Kim, V. S. V., A. Catuneanu, and H.-Y. Kee, Phys. Rev. B **91**, 241110(R) (2015).
- [40] S. M. Winter, Y. Li, H. O. Jeschke, and R. Valentí, Phys. Rev. B **93**, 214431 (2016).
- [41] L. J. Sandilands, C. H. Sohn, H. J. Park, S. Y. Kim, K. W. Kim, J. A. Sears, Y.-J. Kim, and T. W. Noh, Phys. Rev. B **94**, 195156 (2016).
- [42] Y. S. Hou, H. J. Xiang, and X. G. Gong, Phys. Rev. B **96**, 054410 (2017).
- [43] W. Wang, Z.-Y. Dong, S.-L. Yu, and J.-X. Li, Phys. Rev. B **96**, 115103 (2017).
- [44] J. Cookmeyer and J. E. Moore, Phys. Rev. B **98**, 060412(R) (2018).
- [45] T. Suzuki and S.-i. Suga, Phys. Rev. B **97**, 134424 (2018).
- [46] C. Eichstaedt, Y. Zhang, P. Laurell, S. Okamoto, A. G. Eguiluz, and T. Berlijn, Phys. Rev. B **100**, 075110 (2019).
- [47] P. Laurell and S. Okamoto, npj quantum materials **5**, 2 (2020).
- [48] M. Yamashita, J. Gouchi, Y. Uwatoko, N. Kurita, and H. Tanaka, Phys. Rev. B **102**, 220404(R) (2020).
- [49] M. Ye, G. B. Halász, L. Savary, and L. Balents, Phys. Rev. Lett. **121**, 147201 (2018).
- [50] D. A. S. Kaib, S. Biswas, K. Riedl, S. M. Winter, and R. Valentí, Phys. Rev. B **103**, L140402 (2021).
- [51] L. E. Chern, F. L. Buessen, and Y. B. Kim, **6**, 33 (2021).
- [52] S. Koyama and J. Nasu, Phys. Rev. B **104**, 075121 (2021).
- [53] See Supplemental Material at [http://\\*\\*\\*\\*\\*](http://*****) for the detailed methodology and the results of the extended Kitaev-Heisenberg model..
- [54] H. Katsura, N. Nagaosa, and P. A. Lee, Phys. Rev. Lett. **104**, 066403 (2010).
- [55] R. Matsumoto, R. Shindou, and S. Murakami, Phys. Rev. B **89**, 054420 (2014).
- [56] L. Janssen, E. C. Andrade, and M. Vojta, Phys. Rev. Lett. **117**, 277202 (2016).
- [57] G.-W. Chern, Y. Sizuk, C. Price, and N. B. Perkins, Phys. Rev. B **95**, 144427 (2017).
- [58] P. M. Cónsoli, L. Janssen, M. Vojta, and E. C. Andrade, Phys. Rev. B **102**, 155134 (2020).
- [59] T. Yokoi, S. Ma, Y. Kasahara, T. Shibauchi, N. Kurita, H. Tanaka, J. Nasu, Y. Motome, C. Hickey, S. Trebst, and Y. Matsuda, Science **373**, 568 (2021).
- [60] Y.-f. Yang, G.-M. Zhang, and F.-C. Zhang, Phys. Rev. Lett. **124**, 186602 (2020).
- [61] S. M. Winter, K. Riedl, P. A. Maksimov, A. L. Chernyshev, A. Honecker, and R. Valentí, Nature Communications **8**, 1152 (2017).
- [62] K. Ran, J. Wang, W. Wang, Z.-Y. Dong, X. Ren, S. Bao, S. Li, Z. Ma, Y. Gan, Y. Zhang, J. T. Park, G. Deng, S. Danilkin, S.-L. Yu, J.-X. Li, and J. Wen, Phys. Rev. Lett. **118**, 107203 (2017).
- [63] L. Janssen, E. C. Andrade, and M. Vojta, Phys. Rev. B **96**, 064430 (2017).
- [64] J. Cookmeyer and J. E. Moore, Phys. Rev. B **98**, 060412(R) (2018).
- [65] E. C. Andrade, L. Janssen, and M. Vojta, Phys. Rev. B **102**, 115160 (2020).
- [66] X. Hong, M. Gillig, R. Henrich, W. Yao, V. Kocsis, A. R. Witte, T. Schreiner, D. Baumann, N. Pérez, A. U. B. Wolter, Y. Li, B. Büchner, and C. Hess, Phys. Rev. B **104**, 144426 (2021).